DESIGN AND OPTIMISATION OF ROTARY TILLER BLADE FOR ORCHARDS IN HILLY MOUNTAINOUS AREAS BASED ON THE DISCRETE ELEMENT METHOD / 基于离散元法的丘陵山区果园圆盘式开沟刀具设计与优化

Jing MI [1], Huan XIE *[2] Po NIU*[1]
[1]College of Mechanical Engineering, Chongqing Three Gorges University, Chongqing / China.
[2]Chongqing Three Gorges Vocational College, School of Automotive Engineering / China
Tel: +86 17726251480; E-mail: 1478807149@qq.com
Corresponding author: huan xie, Po Niu
DOI: https://doi.org/10.35633/inmateh-76-16

Keywords: *hilly area, orchard, rotary blade, DEM, RSM, optimization*

ABSTRACT
This study investigates the excessive energy consumption of traditional furrowing cutters used in sticky, heavy soils of orchards located in hilly and mountainous regions. A novel furrowing cutter was designed, taking the wetland rotary bending cutter as a reference. The bending radius, bending angle, and alpha angle were selected as design variables. Quadratic orthogonal regression and discrete element method (DEM) simulations were employed to analyse tool–soil dynamic interactions and assess the influence of key parameters on furrowing power consumption. Response surface analysis revealed that at a bending radius of 30.02 mm, bending angle of 109.97°, and alpha angle of 51.74°, the optimised cutter reduced power consumption by 12.9%, from 0.85 kW to 0.74 kW.

摘要
本研究针对丘陵山区果园粘重土壤条件下传统开沟刀具存在的高能耗问题，以湿地旋耕弯刀为参考，设计了一种适用于丘陵山区果园的开沟刀具。通过选择刀具弯折半径、弯折角度和阿尔法角作为控制变量，结合二次正交回归实验和离散元法（DEM）仿真，分析刀具与土壤的动力学交互特性，探讨关键参数对开沟功耗的影响机制。响应曲面分析结果表明，在弯折半径 30.02 mm、弯折角 109.97°、阿尔法角 51.74°的条件下，优化后的刀具功耗由 0.85 KW 降低至 0.74 KW，减少了 12.9%。

INTRODUCTION
Fertiliser application is crucial to fruit tree management, directly influencing yield and quality. Common fertiliser application methods include water-fertiliser integration, open furrow application, and fertiliser spreading, each with inherent limitations. Water-fertiliser integration can cause soil salinisation, while spreading results in fertiliser wastage and lacks precise depth control. Open furrow fertiliser application meets fruit tree nutrient requirements but remains hindered by high energy consumption and low operational efficiency. In China, premium orchards are primarily found in hilly and mountainous regions, including Sichuan, Guangdong, Guangxi, Shaanxi, and Gansu. These areas have low mechanisation levels, with manual labour remaining predominant due to complex terrain and varying soil properties. Given labour shortages and rising costs, developing mechanised furrowing and fertiliser application technologies tailored to complex terrain is increasingly critical *(Asl and Singh, 2009; Chen P. et al., 2024; Fu et al., 2024; Wang et al., 2015)*.

In mechanised furrowing and fertiliser application in orchards, the furrowing tool, as a key component in direct soil contact, plays a crucial role in operational efficiency and power consumption. Extensive research has been conducted globally. *Kang et al., (2017)*, optimised the blade structure, significantly reducing operating power consumption; *QIN et al., (2021)*, proposed a combined cutting and throwing furrowing tool for tea garden mechanisation, effectively enhancing soil-throwing performance; *Barr et al., (2020)*, optimised the tool-soil interaction process using DEM simulation, significantly reducing tool power consumption and providing technical support for optimisation. However, orchard soils in hilly mountainous areas are sticky and heavy, with severe sloughing. The issues of high-power consumption and inefficient furrowing in traditional tools remain unresolved.

Jing Mi, M.S. Stud; huan xie, Assoc. Prof; Po Niu, Assoc. Prof. Ph.D. Eng.

The cutter's structural parameters are critical for enhancing operational efficiency and reducing energy consumption. Inspired by the design of the wetland rotary ploughing curved cutter, this cutter is widely used in wetland and orchard operations due to its superior cutting performance, reduced tangling, and effective soil penetration. Building on these characteristics, this study develops a furrowing cutter tailored for orchard soils in hilly mountainous regions. By optimising the bending radius, bending angle, and alpha angle, soil contact efficiency is improved, and power consumption is reduced.

MATERIALS AND METHODS

Main structure and parameters of furrowing tool

The cutter's structural parameters are essential for enhancing operational efficiency and reducing energy consumption *(Ma et al., 2021; Xiao et al., 2024; Zhang et al., 2022)*. This study adopts the design principles of wetland rotary ploughing curved cutters, which are widely used in wetland and orchard operations for their superior cutting performance, reduced tangling, and effective soil penetration. Building on this concept, a furrowing cutter optimised for orchard soils in hilly mountainous regions was developed. The bending radius, bending angle, and alpha angle were refined to enhance soil contact efficiency and minimise power consumption.

Figure 1 presents a schematic diagram of a furrowing cutter designed based on the wetland rotary ploughing curved cutter concept.

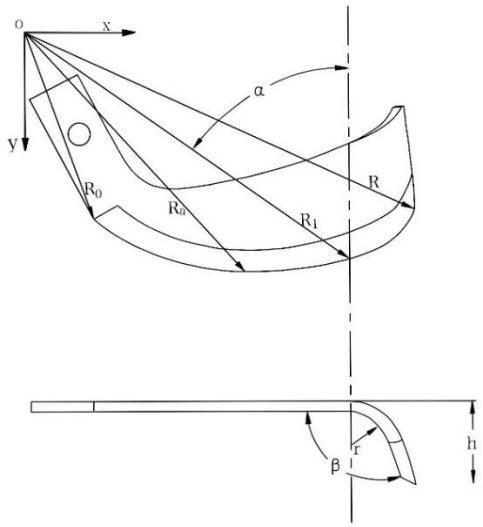

Fig. 1 - Schematic diagram of furrowing tool structure

O - center of rotation, R - radius of rotation, R_0 - radius of the starting point of the side-cutting edge, R_1 - radius of the end point of the side-cutting edge, R_a - radius of any point on the side-cutting edge, α - angle between the radius of the end point of the side-cutting edge and the bend line, r radius of bend, β is the angle of bend, h is the working width.

The main structural parameters of the furrowing tool are shown in Table 1.

Table 1

Main structural parameters of furrowing tool

Parametric	Numerical
Radius of rotation [*R*]	245 [mm]
Radius of the starting point of the side-cutting edge [R_0]	110 [mm]
Radius of the end point of the side-cutting edge [R_a]	220 [mm]
Bending radius [*r*]	45 [mm]
Bending angle [*β*]	135 [°]
Alpha angle [α]	40 [°]
Working width [*h*]	35 [mm]

DEM-based coupled tool-soil modelling

To ensure simulation accuracy, this study selected typical orchard soil from hilly mountainous regions as the simulation environment. The parameters were set based on experimentally measured soil physical properties and supplemented with data from the literature. The soil is primarily compacted clay with fine particles that are difficult to measure directly.

Therefore, reasonable assumptions regarding its physical properties were incorporated into the simulation *(Chen, M. et al., 2024; Chertkiattipol and Niyamapa, 2010; Hao et al., 2023; Wang et al., 2023)*. The Hertz-Mindlin with JKR model was employed to simulate soil particle contact, with a particle size of 5 mm. The simulation parameters for the tool and soil are presented in Table 2.

Table 2

Parameters of the tool-soil coupling model

parametric	numerical	parametric	numerical
Machine forward speed [m/s]	0.3	Soil-soil recovery factor	0.28
Tool speed [rpm]	300	Soil-Fe recovery factor	0.6
Soil density [kg/m³]	2500	Soil-soil static factor	0.5
Poisson's ratio for soil	0.32	Soil-steel static factor	0.5
Soil shear modulus [Pa]	1×10^{6}	Soil-soil rolling factor	0.37
Steel density [kg/m^3]	7850	Soil-steel rolling factor	0.05
Shear modulus of steel [Pa]	7.962×10^{10}	Fe Poisson's ratio	0.3

Lateral cutting-edge curve

During operation, the side-cutting edge vertically cuts the soil, with cutting performance primarily determined by the design of its curve. For furrowing depths of less than 30 cm*(Li et al., 2018)*, the Archimedean spiral is commonly selected as the side-cutting edge curve. Consequently, this study adopts this curve, expressed by the following equation:

$$\rho = \rho_0 + a'\theta \tag{1}$$

ρ_0-polar diameter at the start of the helix, [mm];

a'-increase in polar diameter for every 1 radian increase in the polar angle of the helix, [mm];

θ -arbitrary polar angle on the helix, [°].

To prevent soil compaction by the bladeless section during furrowing, ρ_0 must satisfy the following equation:

$$\rho_0 = \sqrt{R^2 + S^2 - 2S\sqrt{2Ra - a^2}} \tag{2}$$

S - cutting pitch, [mm];

a - furrowing depth, [mm];

R - furrowing knife turning radius, [mm].

The turning radius of the tool is a critical design parameter. Based on the requirements for orchard furrowing in hilly mountainous regions, the maximum gyration radius is set to 245 mm, with a soil-cutting pitch of 30 cm. The pole diameter at the helix's starting point, ρ_0 is calculated as 110 mm.

To ensure a smooth transition between the helix and the tangent edge, the pole diameter at the endpoint, ρ_n is typically 10–20 mm smaller than the gyration radius. Thus, the endpoint pole diameter is designed as 220 mm.

The polar angle θ_n at the helix endpoint is related to the slip shear angle by the following equation:

$$\theta_n = \tan\frac{\rho_n - \rho_0}{\rho_n}\tau_n \tag{3}$$

τ_n-slip angle at the end of the helix, [°].

Considering the requirements of orchards in hilly mountainous regions, the terminal slip cut angle is designed as τ_n=55◦, with a calculated increment of a'=3.14, thereby determining the side-cutting edge helix.

Tangent Curve and Tangent Height

The tangent edge is a spatial curve. To ensure a flat furrow bottom, the curve is positioned on the outer cylindrical surface of the knife stick, where it appears as a circular arc in the side view and transitions smoothly into the side cutting edge *(Fang et al., 2016; Yang et al., 2024)*. In hilly and mountainous orchards, the soil is compacted, requiring the knives to possess soil-breaking capabilities.

Liu et al., (2019), demonstrated that the optimal soil breakage rate and power consumption occurred when the tangent face height was 60 mm. Consequently, in this study, the end face height was set at 60 mm to satisfy the operational requirements of Class I rotary tillage knives. The bending radius, bending angle, and alpha angle influence cutting force and power consumption A smaller bending radius increases efficiency but also friction, whereas a larger radius reduces friction but affects cutting depth. Larger bending angles enhance dispersion efficiency but increase power consumption. The alpha angle influences cutting stability; a smaller angle promotes stable cutting, while a larger angle increases cutting depth but also resistance*(Liu et al., 2024; Zeng et al., 2024)*.

The tool's bending radius r is 30 mm, the alpha angle α is 47°, the bending angle β for the positive cutting part is 120°, the width of the top surface of the side-cutting edge C_1 is 5 mm, and the thickness of the edge C_2 is 1.5 mm.

At this stage, the main dimensional design of the cutter disc-type furrowing tool is essentially complete, and the final three-dimensional representation of the tool is shown in Figure 2.

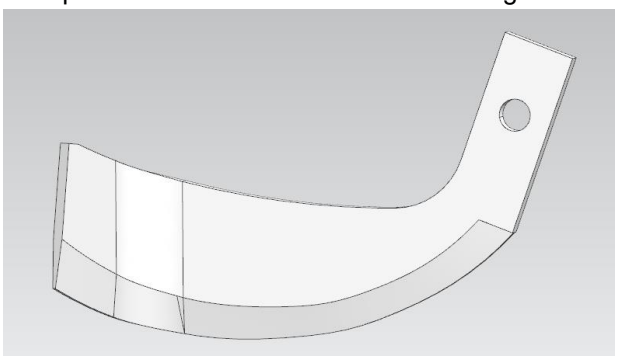

Fig. 2 - Schematic diagram of tool structure

EDEM simulation experiment

The furrowing tool model, based on the tool and soil described in the previous section, is created in UG, saved in STL format, and imported into EDEM. The tool-soil coupling model is then configured according to the physical material properties outlined earlier.

The furrowing tool-soil coupling model, established using the above method and parameters, is shown in Figure 3.

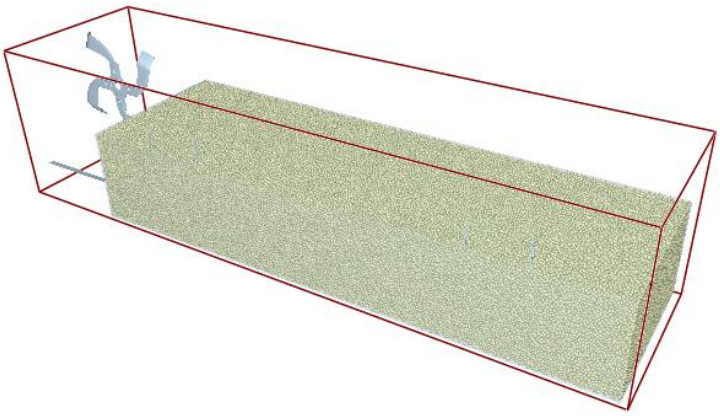

Fig. 3 - Schematic diagram of tool-soil simulation model

As EDEM cannot directly measure the power consumption of the tool, the torque applied to the tool must first be measured and then converted into power consumption using the following formula:

$$P = \frac{T \cdot n}{9549} \quad (4)$$

P - power consumption, [kW];

T - torque, [N·m];

n - tool speed, [rpm].

Quadratic regression orthogonal experimental design

The orthogonal combination design includes a two-level test m_c, asterisk test $2m_\gamma$ and zero-level experiment m_0. The total number of tests, n is calculated using the following equation (*Xiao et al., 2024*):

$$n = m_c + 2m_\gamma + m_0 \quad (5)$$

In accordance with the orthogonality requirement, the arm length parameter, denoted as γ, must satisfy the following relationship:

$$\gamma = \sqrt{\frac{\sqrt{(m_c + 2m + m_0)m_c} - m_c}{2}} \quad (6)$$

The present experiment was a three-factor, two-level full-scale trial, which resulted in $\gamma = 1.353$.

In the context of the given factors, the arithmetic mean is defined as the zero level of factor x_j, denoted x_{j0}, where x_{j2} and x_{j1} represent the upper and lower levels of factor x_j, respectively. Let $x_{j\gamma}$ and $x_{-j\gamma}$ denote the upper and lower asterisk arm levels of factor x_j, respectively. These values correspond to the upper and lower levels of factor x_j.

$$x_{j0} = \frac{x_{j1} + x_{j2}}{2} = \frac{x_{j\gamma} + x_{-j\gamma}}{2} \quad (7)$$

Therefore, the variation in this factor is as follows:

$$\Delta_j = \frac{x_{j\gamma} - x_{j0}}{\gamma} \quad (8)$$

It can be shown that a linear variation in each level of factor x_j leads to the following coding of the levels:

$$z_j = \frac{x_j - x_{j0}}{\Delta j} \quad (9)$$

The factor levels and their corresponding coding results for this experiment are shown in the table 3.

Table 3

Test Factors and Levels

Code	X_1 (Bending radius)	X_2 (Bending angle)	X_3 (Alpha Angle)
γ（1.353）	40	135	52
1	38.6955	131.0864	50.6955
0	35	120	47
-1	31.3045	108.9135	43.3045
$-\gamma$（-1.353）	30	105	42
Δ_j	3.6954	11.0864	3.6954

The test programme and the results obtained from the calculations are presented in the table below.

Table 4

Experimental arrangement and power consumption results

	X_0	X_1 (Bending radius)	X_2 (Bending angle)	X_3 (Alpha Angle)	Y（kW）
1	1	-1	-1	-1	0.837522
2	1	1	-1	-1	0.83587
3	1	-1	1	-1	0.915432
4	1	1	1	-1	0.907356
5	1	-1	-1	1	0.795983
6	1	1	-1	1	0.827545
7	1	-1	1	1	0.832517
8	1	1	1	1	0.883363
9	1	-1.353	0	0	0.850092
10	1	1.353	0	0	0.900149
11	1	0	-1.353	0	0.82978
12	1	0	1.353	0	0.936715

	X_0	X_1 (Bending radius)	X_2 (Bending angle)	X_3 (Alpha Angle)	Y（kW）
13	1	0	0	-1.353	0.891556
14	1	0	0	1.353	0.858958
15	1	0	0	0	0.915705
16	1	0	0	0	0.904034
17	1	0	0	0	0.898701

RESULTS AND DISCUSSION

Analysis of experimental results

Table 5

Analysis of variance

	SS	DF	MS	F-value	P-value	VIF
Model	0.0257	9	0.0029	23.28	0.0002	
A-X_1	0.0017	1	0.0017	13.80	0.0075	1
B-X_2	0.0128	1	0.0128	104.54	＜0.0001	1
C-X_3	0.0035	1	0.0035	28.25	0.0011	1
AB	0.0000	1	0.0000	0.1687	0.6935	1
AC	0.0011	1	0.0011	8.66	0.0216	1
BC	0.0004	1	0.0004	3.32	0.1112	1
A2	0.0024	1	0.0024	19.67	0.0030	1
B2	0.0014	1	0.0014	11.54	0.0115	1
C2	0.0024	1	0.0024	19.52	0.0031	1

Note: P≤0.01 (highly significant), P≤0.05 (significant).

The F-value of the model in the table 5 is 23.28, indicating that the model is significant. The P-value is less than 0.05, further confirming the model's significance. The significant factors include A, B, C, AC, A^2, B^2, and C^2. SS represents the sum of squares, DF is the degrees of freedom, MS is the mean square, and VIF is the Variance Inflation Factor. A VIF value of 1 indicates that the factors are orthogonal. The ANOVA analysis demonstrates that the overall model is significant. The effect of B-X_2 on power consumption is the largest, followed by C-X_3 and A-X_1. Additionally, the interaction between A and C also significantly affects power consumption.

The regression coefficients and goodness of fit can be derived from the ANOVA, and the regression equations are as follows:

$$Y = 0.9069 + 0.0120X_1 + 0.0317X_2 - 0.0178X_3 + 0.0016X_1X_2 + 0.0115X_1X_3 - 0.0093X_2X_3 - 0.0183X_1^2 - 0.0139X_2^2 - 0.0216X_3^2 \quad (10)$$

The results of the significance and confidence analyses for the regression equations are as follows:

Table 6

Confidence analyses of regression equations

Parametric	Numerical
R^2	0.9603
Adjusted R^2	0.9093
P	0.0004

The regression equation had an R^2 of 0.9606 and an adjusted R^2 of 0.9093, with a P-value of 0.0004, indicating that the equation was well-fitted and had a significant effect. The normality of the standardized residuals was verified for the regression model, and these residuals were plotted against the standard distribution, as shown below.

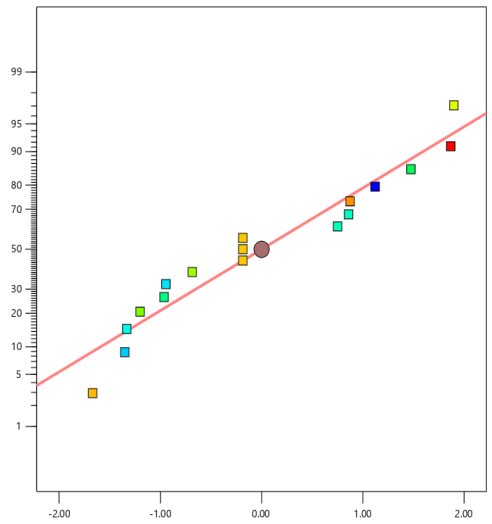

Fig. 4 - Distribution of residual studies

As shown in the Figure 4, the points are distributed along a nearly straight line, indicating that the results are approximately normally distributed. This supports the credibility of the model and aligns with the assumptions of the analysis of variance (ANOVA).

Interaction Effect of Tool Structure Parameters on Power Consumption

In this study, response surface methodology was used to optimise the furrowing tool parameters and analyse the effects of factors and their interactions on power consumption, with the results presented through response surface plots. The response surface of the A (X_1) bending radius and B (X_2) bending angle on power consumption was plotted while keeping the C (X_3) alpha angle at the 0 level. The results show that power consumption increases with the A (X_1) bending radius, with the growth rate slowing at 35 mm and decreasing after reaching a maximum at 36 mm. Power consumption also increases with the B (X_2) bending angle, while it decreases as the C (X_3) alpha angle increases.

The bending radius determines the contact area between the tool and the soil, as well as the force characteristics during the cutting process. A smaller bending radius concentrates the cutting force and reduces the thickness of the soil cutting layer but may result in a larger reaction force. In contrast, a larger bending radius allows the tool to penetrate deeper into the soil, though it may increase power consumption. The bending angle affects both the direction and efficiency of the shear force applied by the tool. Smaller bending angles are suited for shallow cutting but may cause soil build-up and disturbance. Larger bending angles are more suitable for deeper cutting and aid in breaking up compacted layers. The alpha angle influences both the depth of cut and the direction of soil dispersion. Smaller alpha angles enable the tool to cut deeper into the soil but may increase power consumption.

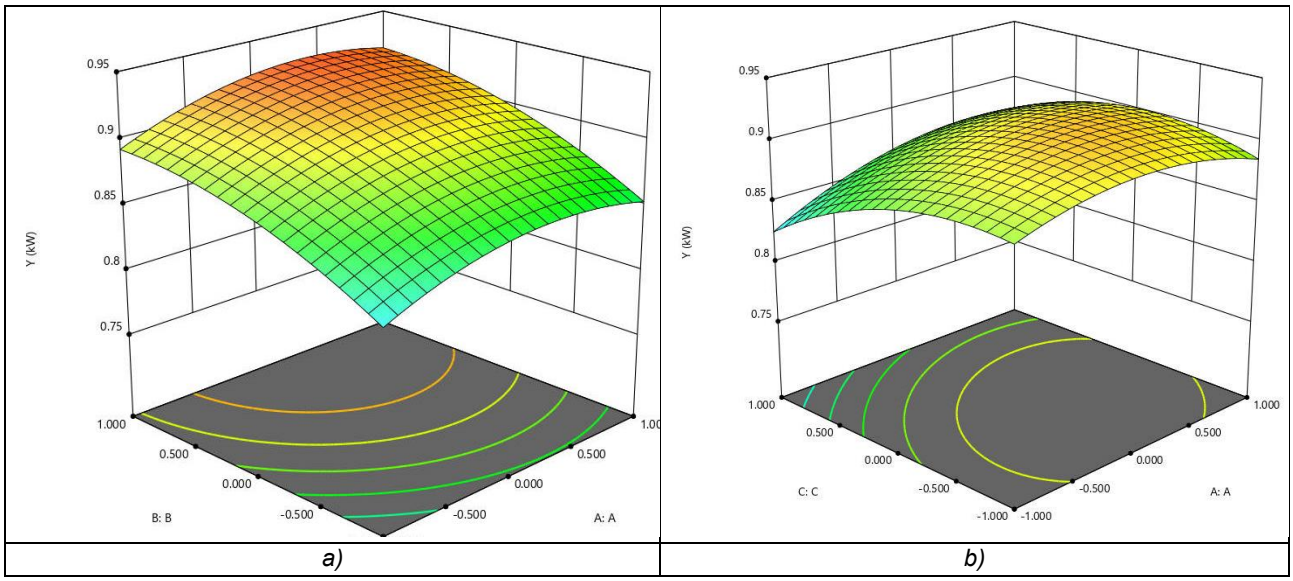

a) *b)*

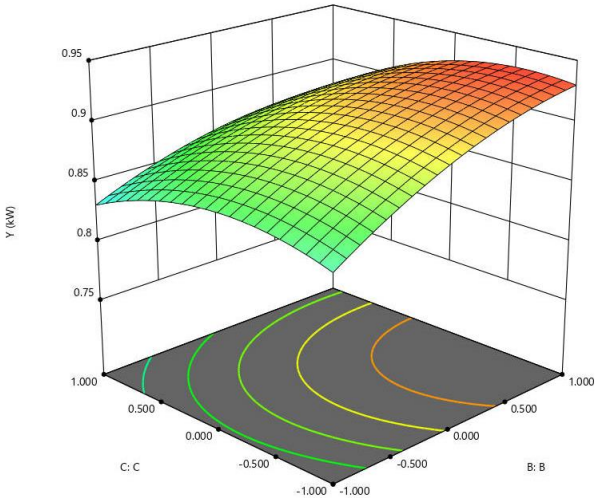

c)

Fig. 5 - Interaction effects of prop structure parameters on power consumption

a) Interaction of X_1 and X_2 on power consumption. b) Interaction of X_3 and X_2 on power consumption. c) Interaction of X_3 and X_1 on power consumption

Analysis of tool optimisation results

The objective of the optimisation is to minimise the furrowing power through the rational selection of tool structure parameters. Consequently, a regression equation was established with the goal of minimising power, to reflect the relationship between tool structure and power consumption, providing a quantitative basis for optimisation.

The constraints for the optimisation process are as follows:

$$\begin{cases} X_1 = [-1.353, 1.353] \\ X_2 = [-1.353, 1.353] \\ X_3 = [-1.353, 1.353] \end{cases}$$

The optimal solution is obtained by solving the following equation:

$$\begin{cases} X_1 = -1.33373 \\ X_2 = -1.19486 \\ X_3 = \ \ 1.21368 \end{cases}$$

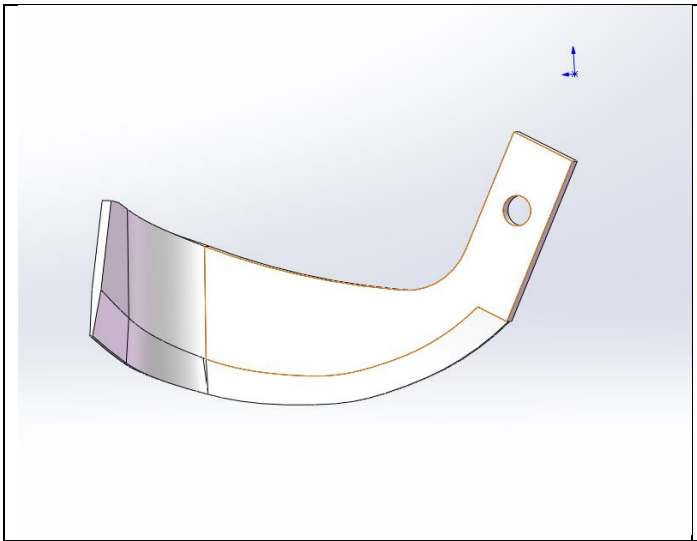

Fig. 6 - Optimised tool model

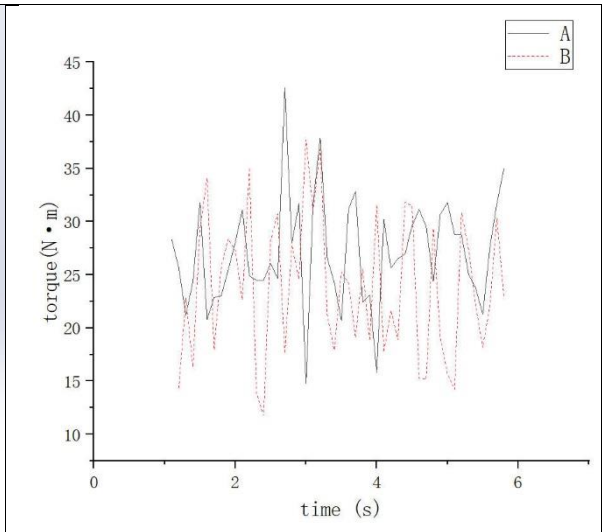

Fig. 7 - Comparison of torque before and after optimization

The optimised furrowing torque graph was generated from EDEM post-processing and plotted using Origin to compare pre-optimisation (torque-A) and post-optimisation (torque-B) values. The results indicate a significant reduction in furrowing torque. After optimisation, the average furrowing torque decreased to 23.90 N·m, while the corresponding furrowing power was 0.75 kW, with a relative error of 1.35%. Compared to the pre-optimisation power of 0.85 kW, furrowing power consumption was reduced by 12.90%.

CONCLUSIONS

This study used a wetland rotary ploughing cutter as a prototype to design a furrowing cutter for orchards in hilly mountainous areas, considering the characteristics of sticky soil. The bending radius, bending angle, and alpha angle of the knives were optimised using quadratic orthogonal regression experiments. The interaction between the knives and soil was analysed through discrete element method (DEM) simulation, with the Hertz-Mindlin with JKR model selected for soil-particle contact modelling. Power consumption during furrowing was used as the evaluation index. Based on the regression analysis and simulation results, the power consumption of the optimised tool is 0.74 kW, 12.9% lower than the pre-optimised value of 0.85 kW. These results demonstrate that by optimally adjusting the tool structure, power consumption can be significantly reduced and working efficiency improved, providing a theoretical basis for the design of orchard furrowing and fertiliser application machinery in hilly mountainous areas.

ACKNOWLEDGEMENT

The work was supported by the Chongqing Municipal Education Commission (KJZD-K202201201), and the Chongqing Wanzhou District Science and Technology Bureau (wzstc20220216), and the Start-up fee for scientific research of high-level talents in Chongqing Three Gorges University (2014/0903341).

REFERENCES

[1] Asl, J. H., & Singh, S. (2009). Optimization and evaluation of rotary tiller blades: Computer solution of mathematical relations. *Soil Tillage Research, 106*(1), 1-7. https://doi.org/10.1016/j.still.2009.09.011

[2] Barr, J., Desbiolles, J., Ucgul, M., Fielke, J. (2020). Bentleg furrow opener performance analysis using the discrete element method. *Biosystems Engineering, 189*, 99-115. https://doi.org/10.1016/j.biosystemseng.2019.11.008

[3] Chen, M., Xu, G., Wei, Y., Zhang, Y., Diao, P., Pang, H (2024). Design and experiment analysis of the small maize harvester with attitude adjustment in the hilly and mountainous areas of China. *International Journal of Agricultural Biological Engineering, 17*(1), 118-127. https://doi.org/10.25165/j.ijabe.20241701.7596

[4] Chen, P., Su, J., Xu, J., Liu, M. (2024). Design and Experiment of Hilly Orchard Vertical Spiral Ditching-fertilizing Machine (丘陵果园立式螺旋开沟施肥机设计与试验). *Transactions of the Chinese Society for Agricultural Machinery, 55*(10), 223-233+274.

[5] Chertkiattipol, S., & Niyamapa, T. (2010). Variations of torque and specific tilling energy for different rotary blades. *International Agricultural Engineering Journal, 19*(3), 1-14.

[6] Fang, H., Ji, C., Zhang, Q., Guo, J. (2016). Force analysis of rotary blade based on distinct element method. (基于离散元法的旋耕刀受力分析). *Transactions of the Chinese Society of Agricultural Engineering, 32*(21), 54-59.

[7] Fu, J., Zhu, J., & Yao, A. I. (2024). The current situation and trend of mechanized ditching and fertilization in hilly and mountainous orchards in China. (我国丘陵山地果园机械化开沟施肥发展现状与趋势). *Agricultural Equipment & Vehicle Engineering, 62*(10), 30-35.

[8] Hao, Z., Zheng, E., Li, X., Yao, H., Wang, X., Qian, S., Li, W., Zhu, M. (2023). Performance analysis of the soil-contacting parts for no-tillage planters and optimization of blade structure. (免耕播种机旋耕刀耕作性能分析与结构优化). *Transactions of the Chinese Society of Agricultural Engineering, 39*(02), 1-13.

[9] Kang, J., Li, S., Yang, X., Liu, L., Wang, C., Liu, X. (2017). Design and Experiment of Ditching Blade Installed in Close Planting Orchard Ditching Machinery. (密植果园开沟施肥机开沟刀片设计与试验). *Transactions of the Chinese Society for Agricultural Machinery, 48*(02), 68-74.

[10] Li, S., Chen, X., Chen, W., Zhu, S., Li, Y., Yang, L., Xie, S., Yang, M. (2018). Soil-cutting simulation and parameter optimization of handheld tiller's rotary blade by Smoothed Particle Hydrodynamics modelling and Taguchi method. *Journal of Cleaner Production*. https://doi.org/10.1016/j.jclepro.2017.12.228

[11] Liu, M., Liu, Y., Ku, H., Chen, L., Wang, J., Xie, B. (2019). Research on the Cutting Performance of Ridger Based on Discrete Element Method. (基于离散元法的筑埂机旋耕切削性能研究). *Journal of Agricultural Mechanization Research, 41*(10), 129-134+140. doi:10.13427/j.cnki.njyi.2019.10.024

[12] Liu, M., Xie, F., Liu, D., Wang, X. (2024). Analysis and experiment of the power of blade roller in reverse-rotary ditching machine based on the granular scale effect. (基于颗粒放尺效应的逆旋开沟机刀辊功耗分析与试验). *Transactions of the Chinese Society of Agricultural Engineering, 40*(07), 83-92.

[13] Ma, C., Qi, J., Kan, Z., Chen, S., Meng, H. (2021). Operation power consumption and verification tests of a trenching device for orchards in Xinjiang based on discrete element. *International Journal of Agricultural Biological Engineering, 14*(1), 133-141.

[14] Qin, K., Liang, X., Cao, C., Ding, W., Wu, Z., Fang, L. (2021). Design and Experiment of Combined Cutting and Throwing Ditching Blade for Tea Garden. (茶园切抛组合式开沟刀设计与试验). *Transactions of the Chinese Society for Agricultural Machinery, 52*(05), 74-82.

[15] Wang, F., Qiu, Z., Pan, Y., Sun, G. (2023). DEM-based parameter optimization and tests of digging green onions. *International Journal of Agricultural Biological Engineering*

[16] Wang, P., Li, G., Li, S., Wu, X., Cao, Z., Chen, J. (2015). The Research Situation and Development Ideas of Orchard Ditcher in China (我国果园开沟机的研究现状与发展思路). *Agricultural Equipment & Vehicle Engineering, 53*(07), 30-33.

[17] Xiao, W., Niu, P., Wang, P., Xie,Y., Xia, F. (2024). Simulation analysis and optimization of soil cutting of rotary blade by ANSYS/LS-DYNA. *INMATEH-Agricultural Engineering, 72*(1), 22-32. DOI: https://doi.org/10.35633/inmateh-72-02

[18] Yang, D., Cai, W., Wu, R., Zhang, X., He, Y. (2024). Optimization design of structural parameters for rotary tiller blade of tea garden micro tiller based on discrete element method. (基于离散元法茶园微耕机旋耕刀结构参数优化设计). *China Southern Agricultural Machinery, 55*(01), 7-10+15.

[19] Zeng, Y., Jiang, X., Wu, M., Tang, L., Li, P. (2024). Development of the layered cut and throw ditching blade groups for oil tea forest based on DEM-MBD. (基于 DEM-MBD 的油茶林分层切抛式开沟刀组研制). *Transactions of the Chinese Society of Agricultural Engineering, 40*(08), 30-42.

[20] Zhang, X., Zhang, L., Hu, X., Wang, H., Shi, X., Ma, X. (2022). Simulation of soil cutting and power consumption optimization of a typical rotary tillage soil blade. *Applied Sciences, 12*(16), 8177.